ICESat-2 Atmospheric Channel Description, Data Processing and First Results

Stephen P. Palm[1], Yuekui Yang[2], Ute Herzfeld[3], David Hancock[1], Adam Hayes[3], Patrick Selmer[1], William Hart[1] and Dennis Hlavka[1]

[1]Science Systems and Applications, Inc., Lanham, MD, 20706
[2]NASA Goddard Space Flight Center, Greenbelt, MD 20771
[3]University of Colorado, Boulder, CO 80309

Corresponding author: Stephen P. Palm (stephen.p.palm@nasa.gov)

Key Points:

- ICESat-2 is a satellite lidar optimized for altimetry but also acquires atmospheric backscatter profiles from 0 – 14 km every 280 m along the satellite track.
- The high repetition rate laser used by ICESat-2 creates unusual problems for processing the raw data to higher level data products that require innovative solutions.
- Higher level products such as calibrated backscatter, cloud and aerosol layer heights, column optical depth and blowing snow are described and examples shown.

Plain Language Summary:

ICESat-2 is a polar orbiting satellite equipped with a high repetition rate laser that fires green pulses of light to earth 10,000 times per second. The main objective of ICESat-2 is the high-resolution measurement of the height of the earth's surface, with emphasis on the change in elevation of ice sheets that cover most of Greenland and Antarctica. In addition to surface elevation, ICESat-2 also obtains information on the vertical structure of the atmosphere including the height and thickness of clouds and aerosols. The atmospheric measurements are important for climate studies and because they extend the data record begun by other earth-orbiting satellite lidars like CALIPSO which has been acquiring atmospheric data since 2006 and is nearing the end of its life. The creation of a long record of cloud and aerosol observations is

very important for detecting changes that may be occurring due to humanity's influence on the climate system.

Abstract

The Advanced Topographic Laser Altimeter System (ATLAS) was launched aboard the Ice Cloud and land-Elevation Satellite-2 (ICESat-2) satellite in September 2018. ATLAS is a single wavelength (532 nm) lidar system designed to acquire high resolution measurements of the earth's surface while also obtaining atmospheric backscatter from molecules, clouds, and aerosols. Because ATLAS is optimized for altimetry, the atmospheric data acquired is unique in many respects and requires non-standard analysis techniques. For example, the high repetition rate laser limits the vertical extent of the profiles to just 14 km and causes atmospheric scattering from above 15 km to be added to the scattering in the lower 0 -14 km profile. In addition, the limited vertical range of the acquired profiles renders it difficult to compute the magnitude of the solar background and hinders the application of standard calibration techniques. Despite these limitations, techniques have been developed to successfully produce data products that have value to the atmospheric community for cloud and aerosol research and are currently available at the National Snow and Ice Data Center (NSIDC). In this paper we describe the ICESat-2 atmospheric channel and the methods used to process the ATLAS raw photon count data to obtain calibrated backscatter and higher level products such as layer heights and type, blowing snow, column optical depth and apparent surface reflectance.

1 Introduction and Background

The Ice, Cloud and land Elevation Satellite (ICESat), which operated from 2003 until 2009 was the first satellite lidar to study the earth's surface and atmosphere (Spinhirne et. al., 2005). ICESat-2, the successor to ICESat, was launched into a 92° inclination orbit in September of 2018 and has been in continuous operation since October of that year (Abdalati et al., 2010; Markus et al., 2017). Though specifically designed and optimized to obtain high resolution altimetry measurements of the Earth's surface, ICESat-2 also has an atmospheric channel to record backscatter from clouds and aerosols from 14 km altitude to the surface. ICESat-2 carries only one instrument – the Advanced Topographic Laser Altimeter System (ATLAS) that utilizes a high repetition rate (10 KHz), low per pulse energy (375 μJ), 532 nm laser and photon counting detectors. Table 1 lists the ATLAS instrument specifications. ATLAS employs a diffractive optical element (DOE) to split the laser pulse into 6 individual beams that are simultaneously emitted from the satellite. Three of the beams have nominal energies of about 25 μJ per pulse (weak beams) and the other 3 have energies roughly 4 times the weak beams (strong beams). The altimetry measurements utilize all 6 laser beams while for the atmospheric measurements, backscatter data are captured only from the 3 strong beams (known as profile1, profile2 and profile3 on the ATL04 and ATL09 data products). Each strong/weak beam pair is separated by about 3 km on the ground (across track) as shown in Figure 1.

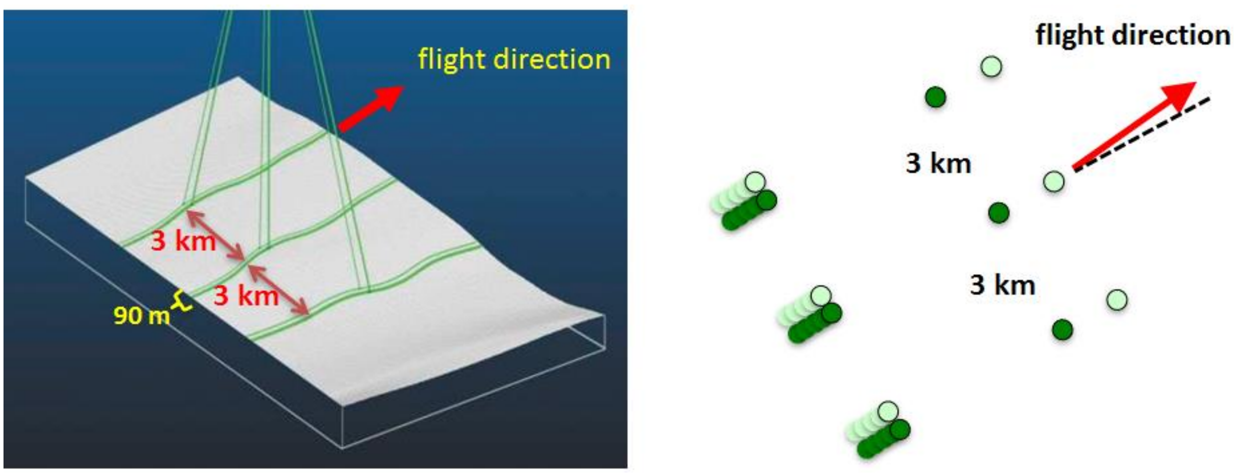

Figure 1. ICESat-2 laser beams and surface tracks. The satellite is yawed by 2 degrees such that the weak beams trail the strong beams and vice versa depending on spacecraft orientation which is determined by solar beta angle. Separation of strong and weak beam tracks is 90 m on the ground and beam pairs are separated by 3 km.

The three ICESat-2 atmospheric profiles consist of 30 m bins in a 14 km long column. Nominally the top of the column is about 13.75 km (above the local value of the onboard Digital Elevation Model (DEM)) and the bottom -0.250 km. This vertical region captured by the instrument is called the atmospheric range window (ARW). Because of various altimetric calibrations that occur over mainly sea ice, the ARW can deviate from the nominal value in these regions. For instance, over the arctic the top of the ARW can at times be as low as 12 km and the bottom 2 km below the surface. For the atmosphere, the 3 strong beams (approximately 100 μJ at 532 nm) are downlinked after summing 400 shots onboard the satellite, resulting in three 25 Hz profiles (280m along track resolution). Thus, each summed, 25 Hz profile is equivalent to roughly 40 mJ of energy (400 shots x 0.1 mJ/pulse), which is about twice the level of each ICESat/GLAS (Geoscience Laser Altimeter System) 532 nm single shot (40 Hz) profile and about half of the per pulse (20 Hz) laser energy of the Cloud-Aerosol Lidar and Infrared Pathfinder Satellite Observations (CALIPSO) 532 nm channel.

ATLAS uses low dark current (<10 KHz), photon counting detectors (one for each laser beam) with a 3 ns dead time, thus providing very good nighttime data. A unique feature of the ATLAS instrument is its in-flight, continuous boresight alignment system. The Telescope Alignment Monitoring System (TAMS) is the first of its kind for a satellite lidar. By picking off a small portion of outgoing laser energy and received signal, the TAMS keeps the transmitted beam centered in the telescope field of view (Martino et. al., 2019). This is a major advance over prior satellite lidars and helps to maximize the received signal thereby keeping the system calibration more stable than previous satellite lidar systems. The main ATLAS instrument specifications are given in Table 1.

Table 1. ATLAS instrument specs

ATLAS Instrument Parameter	Nominal Value
Laser Repetition Rate	**10 KHz**
Laser Energy (strong; weak)	**100; 25 μJ**
Telescope Effective Area	**0.43 m^2**
Telescope FOV	**83 μr**
Detector Quantum Efficiency	**0.15**
Detector Dead Time	**3 ns**
Detector Dark Count Rate	**1-10 KHz**

Bandpass Filter Width	**30 pm**
Receiver Transmission	**0.40**
Nominal Orbit Height	**495 km**
Orbit Inclination; Repeat	**92°; 91 days**
Laser/Telescope FOV Spot Size (on ground)	**17 m/ 45 m**

The use of a high rep rate, low per pulse energy laser introduces a number of negative consequences for the atmospheric measurements. At 10 KHz, each laser pulse is separated in the vertical by just 30 km. This means that the atmospheric return from a laser pulse at height z will return to the receiver on the satellite at the same time as the return from the next laser pulse at height z+15 km. Stated more generally, the atmospheric backscatter recorded by ATLAS at height z is the sum of the backscattering at heights z, z±15 km, z±30 km, z±45 km, etc. This effect, heretofore termed folding, will cause the returns from 2 km altitude, for example, to be combined with those from 17 km. Thus, for instance in the tropics, clouds between 15 – 18 km are folded down to 0-3 km, adding to the scattering that is present there and making them indistinguishable from what is actually in the atmosphere in the 0 - 3 km altitude range. Thankfully, clouds occurring above 15 km are generally limited to tropical regions (aside from polar stratospheric clouds). Note also that molecular scattering from above 15 km is also folded down into the acquired ATLAS profile. This, unlike particulate scattering, can be modeled and removed from the profile (this is discussed in section 3). Another detrimental factor for atmospheric measurements when using a high repetition rate laser is the solar background noise. When summing signals over a fixed time interval, the solar noise in a lidar system scales with the laser repetition rate. Thus, a laser such as used in ICESat-2 will produce lower daytime signal quality than a system with equivalent laser power but lower repetition rate, all else being equal.

The fact that ATLAS provides only a 14 km profile also makes it very difficult to compute the magnitude of the solar background from the data because there is no region in the profile that is devoid of atmospheric signal. In low repetition rate satellite lidar systems such as CALIPSO (20 Hz) or GLAS (40 Hz), the vertical extent of the profile is 40 km or more with many km of data below the ground. The background can be calculated from data either very high up in the atmosphere or below the ground. ATLAS is unable to capture data in these regions and the background must be estimated from data only within the 14 km profile (how this is done is explained further in the next section). The limited 14 km profile of ATLAS also produces problems when trying to calibrate the data. In other satellite lidar systems this is done by normalizing the signal to the scattering from a portion of the atmosphere known to be devoid of particulates. Usually this would be in the mid to upper stratosphere (CALIPSO for instance uses the 35-40 km region). ATLAS does not provide access to this region and alternative methods for calibration must be employed.

The intent of this paper is to provide information about the ICESat-2 instrument and atmospheric measurements, describe some of the atmospheric parameters in the publicly available data products and present preliminary results. Sections 2 and 3 describe how the solar background is calculated and subsequent normalized relative backscatter is produced. Calibration of the data is discussed in section 4 and the layer detection algorithm and cloud-aerosol discrimination are described in section 5. Section 6 describes the blowing snow algorithm and section 7 discusses Apparent Surface Reflectance and how it can be used for estimating total column optical depth and cloud detection. A summary and concluding remarks are in section 8.

2 Solar Background Computation

As discussed in the introduction, there is no ideal place to compute the solar background from the ATLAS data as it must be computed from the 14 km profile. The method used to compute the background (ATL09 parameter *back_c*) depends on the solar elevation angle. If the solar elevation angle is less than -7 degrees (nighttime), the background is not computed from the data. Instead, a constant value is used for the background (0.0604 photons/bin) which was determined through a trial and error process after launch. For solar elevation angles between -7.0 and -1.0 (twilight), the background is computed from the average of the bottom 400 m of the profile times a factor that depends on the cosine of the solar elevation angle. For daytime data (solar elevation > -1.0), the profile is divided into 6 equal length segments and the average signal for each is computed. The background is set to the minimum segment average. The twilight background computation is causing calibration issues (for the twilight data) and efforts are underway to fix that problem. The daytime background computation seems to work well, but it is possible that the computed background is too large as evidenced by the need for a negative alpha value in the molecular folding correction (discussed in the next section). A negative alpha value essentially adds signal to the background subtracted profile, which is consistent with the computed background being too large. More detail on the background computation can be found in Palm et al., (2020).

3 NRB Computation

After the background has been estimated from the raw photon count data, the normalized relative backscatter (NRB) is computed (reported on the ATL04 product, parameter *nrb_profile*). In this step, three corrections to the data are made: 1) Laser energy normalization, 2) range square correction and 3) background subtraction. The lidar equation is:

$$S(z) = \frac{CE\beta(z)T^2(z)}{r^2} + p_b + p_d \qquad (1)$$

In equation 1, r is the range from the spacecraft to the height z, $S(z)$ is the measured raw signal (photons) at height z, C is the lidar system calibration coefficient, E the laser pulse energy, $\beta(z)$ the 180° backscatter coefficient at height z, $T(z)$ the one way atmospheric transmission from the spacecraft to height z, p_b the solar background and p_d the detector dark count rate. For daytime data, the latter is much, much smaller than the solar background and can be neglected. The NRB (computed for each of the 3 strong beams) is then:

$$NRB(z) = (S(z) - p_b)r^2/E \ = C\beta(z)T^2(z) \qquad (2)$$

Where r is the distance from the satellite to the height z. Equation 2 is the standard way to compute NRB, but as mentioned in the introduction, the raw photon data captured by ATLAS at height z will have contributions from atmospheric scattering at height z+15 km, z+30 km, z+45 km, etc. There will be particulate and molecular scattering contributions, but there is very limited knowledge of the former. However, the latter can be modeled and removed from the recorded profile. A similar procedure was used to correct molecular folding in CATS data (Pauly et al., 2019). The molecular contribution to the received photon count can be computed from equation 3:

$$P_m(z) = \frac{E}{r^2}\beta_m(z)\Delta z A_t T_m^2(z) T_o^2(z) S_{ret} N_a R(z)\alpha \tag{3}$$

In equation 3, α is used to adjust the computed photon count since all the terms in equation 3 are not known to sufficient accuracy. The other terms used in equation 3 are:

E – The laser energy in Joules
r – The range from the satellite to the height z (in m).
$\beta_m(z)$ – the molecular backscatter cross section at height z ($m^{-1}\ sr^{-1}$).
Δz – the bin size in meters (30 m)
A_t – Area of telescope (m^2, effective)
$T_m(z)$ – Molecular atmospheric transmission from top of atmosphere to height z.
$T_o(z)$ – Ozone transmission: top of atmosphere to height z
S_{ret} – Receiver return sensitivity (photons/J)
N_a – Number of shots summed (nominally 400)
$R(z)$ – aerosol scattering ratio (nominally 1.02)

Equation 3 is used to compute a profile of received photons due solely to molecular scattering from 60 km to 0 km ($P_m(z)$). From that profile, the molecular scattering contribution (folded from above) to the measured ATLAS photon profile is computed as:

$$P_m'(z) = P_m(z+15) + P_m(z+30) + P_m(z+45) \quad (4)$$

For z between -1 and 20 km. Note that this quantity is computed up to 20 km since the raw profile is being captured 14 km above the value of the DEM at the satellite location, and there will be times (which occur over elevated terrain) when the values between 14 km and 20 km are needed. Note also, the height in the third term in Equation 4 will go above 60 km for z > 15 km. This is above the top height of the input meteorological data (60 km). The values of $P_m(z)$ for z > 60 are set to $P_m(60)$.

Then the corrected raw photon count profile is:

$$S'(z) = S(z) - P_m'(z) \quad (5)$$

Where $S(z)$ is the raw photon count profile measured by ATLAS. Note that this process leaves the molecular scattering of the original profile ($S(z)$) intact. It only removes the molecular scattering folded down from above. The NRB corrected for the molecular folding can now be computed as:

$$NRB'(z) = (S'(z) - p_b)r^2/E = C\beta(z)T^2(z) \quad (6)$$

Since we may not know all the instrument parameters accurately, or they may drift somewhat with time, a scale factor (α) is used in equation 3. If we knew all instrument parameters perfectly the value of α would be 1 but is in practice not unity. The main practical effect of the procedure to remove the molecular folding is on the slope of the average clear-air calibrated profile. If the amount of subtracted folding is too large, the slope of the average clear-air signal will be greater than the slope of the average molecular profile. If alpha is too small, the slope of the average clear-air signal will be less than the slope of the average molecular profile. This same clear-air signal slope behavior is seen in non-high rep rate lidar systems when too little or too much background is removed from the raw signal. Since it is very difficult to measure the background in ATLAS profiles, the molecular folding removal procedure is also a way to correct for imprecise knowledge of the background. Values of alpha are obtained for each of the 3 ATLAS profiles separately by plotting many cases of clear-air average profiles together with the average molecular profiles and adjusting alpha until the two slopes match. This is done for night, day, and twilight cases, resulting in distinct alpha values for the 3 solar regimes. For profile1 alpha values in use for release 003 are 4.7, 1.5 and -3.8 for night, twilight and day, respectively. The alpha values for the other two profiles are similar.

4 Calibrated Attenuated Backscatter

To obtain the calibrated, attenuated backscatter profiles (ATL09 parameter *cal_prof*) the system calibration coefficient must be determined (ATL09 parameter *cal_c*). As mentioned in the introduction, the active boresight system keeps the laser footprint within the telescope field of view (TAMS). Calibration changes in a satellite lidar system are due in large part to the laser spot drifting partially outside of the telescope field of view (FOV). This often happens as a result of thermal changes as the satellite goes from night to day and vice versa. Despite the very narrow field of view of the ATLAS telescope (83 μr), the TAMS is able to keep the laser spot within the telescope FOV, keeping the calibration stable, which is indeed very fortunate for the atmospheric data processing. In fact, the calibration is so stable that the change in nighttime calibration was less than 10% from October 2018 to March 2020. For the release 002 data products, three calibration constants were used: one each for daytime, nighttime and twilight conditions. While this worked well for the nighttime data, the calibration was more variable during daytime and twilight. Especially in areas of high solar background, the data were not well calibrated using a single, constant calibration value for all the daytime data.

In an effort to improve the daytime calibration, a new algorithm was designed to compute the calibration continuously over the orbit. The method, which will only be summarized here (for details consult Palm et al., 2020), entails computing the average NRB signal between 11 km and the top of the profile (usually ~14 km) for roughly two-minute long segments. Each two-minute NRB average is used only if it falls within a narrow pre-defined NRB range. This range is determined from visual inspection of images to identify clear regions and then computing the average NRB in those regions. This is done for day, night and twilight portions of the orbit yielding NRB range limits for those three solar regimes. After all segment averages have been computed, the calibration constant is computed for each segment as:

$$C = \overline{NRB'(z_C)} / [(\overline{\beta_m(z_c)} T^2(z_c) R(z_c)] \qquad (7)$$

Where $\beta_m(z_c)$ is the attenuated molecular backscatter (in the 11-14 km altitude), $T^2(z_c)$ is the two way transmission from the top of the atmosphere to the height z_c, taken to be 12.5 km. $T^2(z_c)$ in equation 7 is composed of molecular transmission, ozone transmission, $T^2_o(z_c)$, and the transmission loss due to particulates, $T^2_p(z_c)$ from the top of the atmosphere to height z_c.

$$T^2(z_c) = T^2_m(z_c) T^2_p(z_c) T^2_o(z_c) \qquad (8)$$

$T^2_p(z_c)$, the particulate transmission term is not known exactly and must be estimated from climatology. We have elected to use the value of 0.95 but realize that this can be highly varying in space and time. In equation 7, the *R* factor is the aerosol scattering ratio within the calibration region with a nominal value of 1.08. Each calibration value is then checked to see if it falls within an allowable range specified for each solar regime. If it is outside of the allowable range, the calibration value is set to a default value. The calibration value between the segments is computed by piecewise-linear interpolation from one segment to the next at one second resolution. Finally, the calibration values before the first and after the last NRB average segments are set to the calibration values computed from the first and last segment values, respectively. The same calibration value is used for each of the 25 profiles within a second. This process is performed on each granule independently, with no attempt to smoothly join calibration values from one granule to the next.

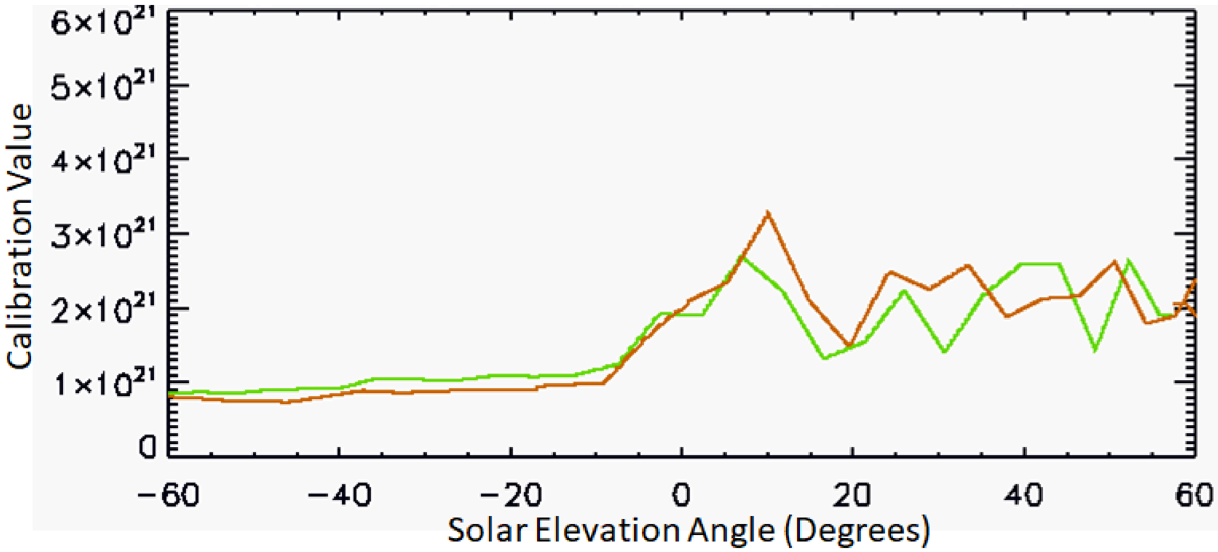

Figure 2. Typical calibration values for profile1 for one complete granule (orbit) as a function of solar elevation angle. The green line is the first half of the orbit which begins near 60° solar elevation and continues toward smaller solar elevation angles, ending at -60°. The red line is the second half of the orbit and begins at a solar elevation angle of -60° and ends at 60°. Data are from granule ATL09_20190131175333_05240201_003_01.h5.

Figure 2 is a plot of the calibration values for one complete orbit. The values shown are for profile1 but the curves for the other two profiles are very similar. The nighttime calibration has an average value of about 0.95×10^{21} and is very stable and repeatable from one granule to the next. Note, interestingly, that the second half of the time the satellite spends in the earth's shadow, the smaller the calibration (i.e. the red line is lower than the green line). This behavior is observed for all orbits and indicates a slight thermal dependence on the calibration (i.e. a smaller calibration value as the spacecraft cools). As the solar elevation angle becomes greater than about -8°, solar background as seen by the instrument starts to become significant. At that point the calibration value begins to increase, gradually obtaining an average daytime value of about 2.0×10^{21}, but now with considerable variability. The increase in magnitude and variance of the calibration can likely be explained in two possible ways: 1) the increased flux of photons hitting the detectors cause heating and a change in detector responsivity (this was seen in ICESat/GLAS), or 2) the inability to effectively remove cloud and aerosol from the calibration zone (11-14 km) when computing the average NRB due to the higher daytime noise. This would result in NRB values that are too large and at least partially explain the increased magnitude and variability of the computed calibration values. One might ask whether the fluctuations in the daytime calibrations are real. Counterintuitively we have found that high background regions have a lower calibration value than low background regions. We have checked the daytime calibration for many cases by plotting the average calibrated backscatter and molecular backscatter in clear regions (examples shown in Figure 3) and have generally seen that the daytime data are well calibrated (to about 20 percent). This new calibration method was utilized to produce the release 003 calibrated, attenuated backscatter profiles on the ATL09 data product which was made public in April 2020. Currently we are working to improve daytime and twilight calibrations for the next release (004), which will be available early 2021.

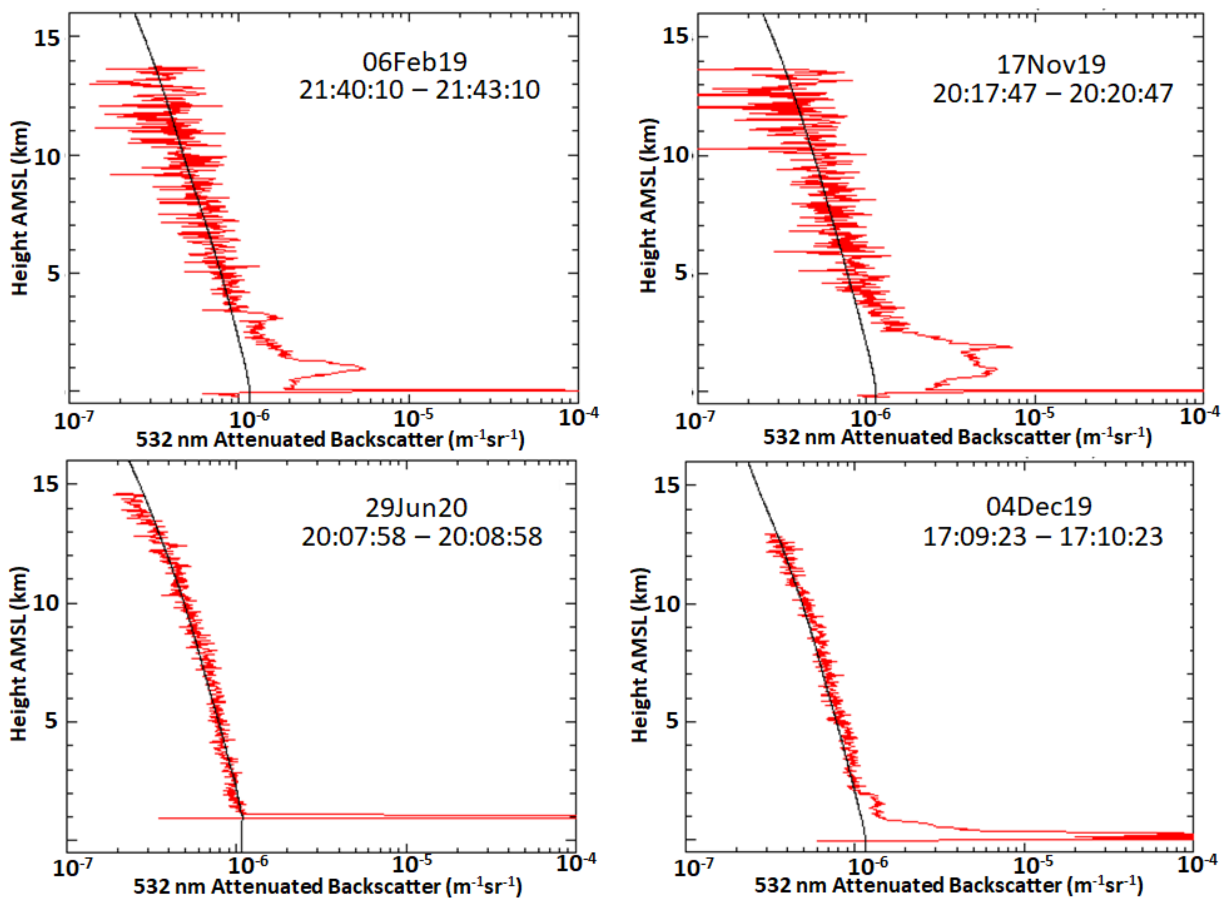

Figure 3. Examples of average ICESat-2 calibrated attenuated backscatter plotted with the corresponding average attenuated molecular backscatter (black line) for various clear-air cases. The top row is daytime, 3 minute averages and the bottom row nighttime, 1 minute averages.

4.1 Calibration Validation

In the Fall of 2019, the Cloud Physics Lidar (CPL) (McGill et al., 2002) on the NASA ER-2 aircraft was flown beneath ICESat-2 to acquire correlative measurements of calibrated, attenuated backscatter. This flight occurred on October 29, 2019 off the coast of California. The data are shown in Figure 4 where the CPL data are on the bottom and the ICESat-2 data on top. Both images show the presence of smoke from the Fall, 2019 Sonoma fires above the marine boundary layer. The point of exact coincidence between aircraft and satellite is denoted by the vertical white line drawn through both images. On the right, a 10 second average of the calibrated, attenuated backscatter profile centered around the coincident point from ICESat-2 (green) and CPL (red) is plotted. Also plotted is the attenuated molecular backscatter (black). This analysis reveals that the ICESat-2 data are very well calibrated with respect to both molecular and the CPL. The ICESat-2 data shown are from the release 003 ATL09 data product, which has improved calibration compared to prior releases.

The Cloud-Aerosol Lidar and Infrared Pathfinder Satellite Observations (CALIPSO) mission (Winker et. al., 2009) continues to acquire high quality measurements of clouds and aerosols since its launch in 2006. While the orbits of ICESat-2 (precessing), and CALIPSO (sun-synchronous) are different, they of course cross frequently. Occasionally they cross at nearly the same time, giving the opportunity to compare the two in a meaningful way. Figure 5 shows one such case that occurred over south-central Australia on November 24, 2018 at roughly 16:10 UTC (local time 1:40 AM November 25). The map on the right shows the tracks of the two satellites (red for ICESat-2) that crossed within 2 minutes of each other. The corresponding images of attenuated, calibrated backscatter are shown on the left, with the red line drawn on the images indicating the crossover point.

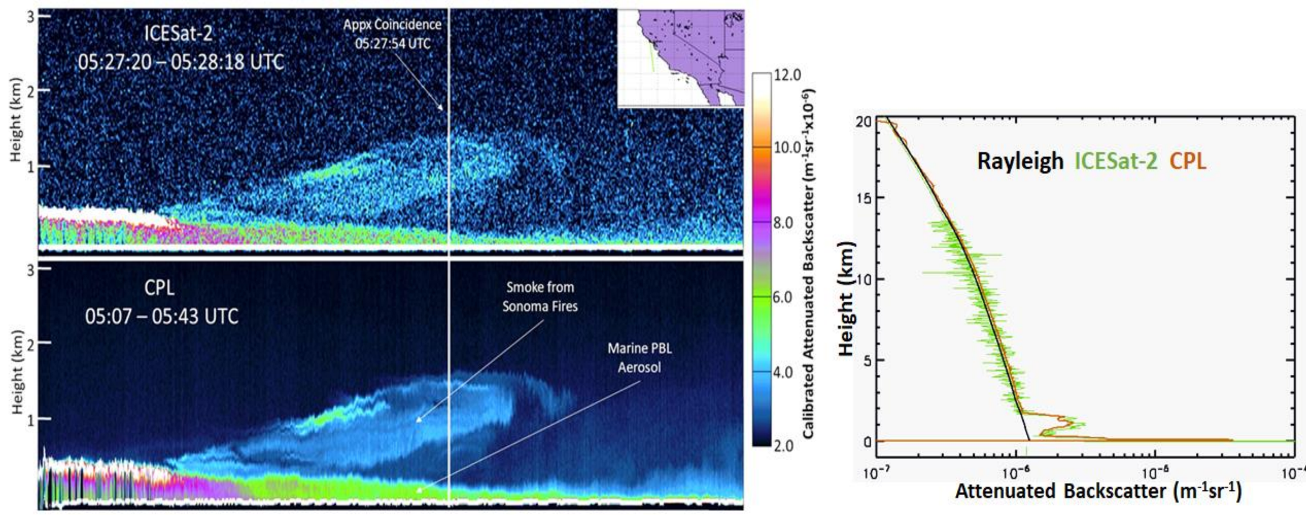

Figure 4. Top: ICESat-2 calibrated, attenuated backscatter (CAB) for a short segment off the coast of California, on October 29, 2019. Bottom: Cloud Physics Lidar (CPL) CAB along the same segment at nearly the same time. Exact temporal and spatial coincidence is indicated by the vertical white line through the images. Right: The 10 second average signal centered on coincidence for ICESat-2 (green) and CPL (red). ICESat-2 data are from granule ATL09_20191029054405_04940501_003_01.h5

The images in Figure 5 demonstrate that the quality of the ICESat-2 nighttime data are as good or better than CALIPSO. The average calibrated, attenuated profile was computed from the data between the white lines drawn on the images (roughly 50 seconds) and is shown in the plot on the right (red ICESat-2, black CALIPSO). Also shown on this plot is the attenuated 532 nm molecular backscatter (green line). The CALIPSO and ICESat-2 average signals around the crossover point agree very well with each other, especially in the clear air above 2 km, with both closely following the attenuated molecular backscatter curve. In the aerosol layer below 2km, the ICEsat-2 signal is somewhat larger than CALIPSO's but this could be due to the spatial and temporal differences between the two measurements.

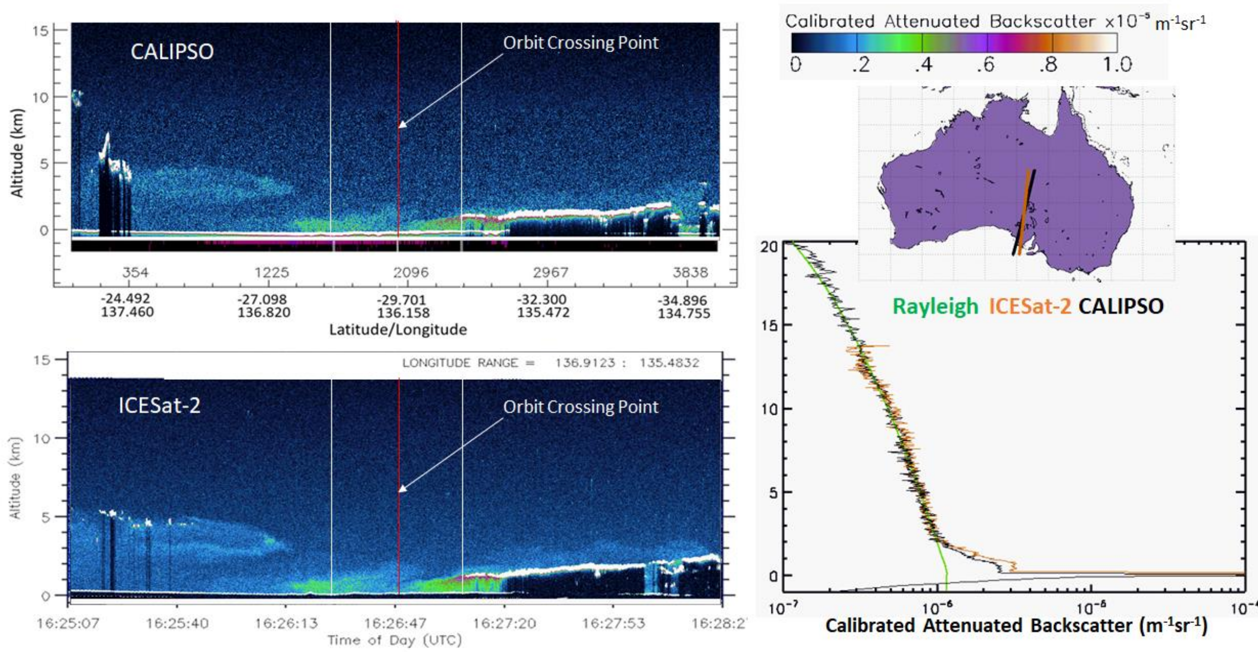

Figure 5. Top: ICESat-2 CAB along the red track on the map in the upper right. Bottom: CALIPSO CAB along the black line on the map. The crossing point of the two tracks is indicated by the vertical red line on both images and occurs within 2 minutes of each other. Right: The average ICESat-2 (red) and CALIPSO (black) CAB profiles computed between the two vertical white lines on the images plotted with the attenuated molecular profile (green line). ICESat-2 data are from granule ATL09_20181124153202_08710101_003_01.h5 and CALIPSO data are from granule CAL_LID_L1-Standard-V4-10.2018-11-24T17-24-59ZN.hdf

In addition to Figures 4 and 5 that demonstrate the nighttime calibration accuracy of ICESat-2, we have continually checked the calibration by comparing the average signal in very clear regions to molecular backscatter for random granules since launch. Examples of such comparisons are shown in Figure 3 for both day and night. As a general rule, the calibration is very good at night. Based on those analyses and CALIPSO and CPL comparisons, we estimate the error in nighttime calibration to be less than 10%. The accuracy of daytime calibration is harder to assess, as there are no correlative measurements from CPL and we have not yet used CALIPSO to compare. However, based on our clear air, multi-granule analyses, the daytime calibration error can be as large as 20-30% but is generally less than that. The daytime calibration has the highest error in areas of very high background caused by clouds or snow-covered surfaces.

Another way to check the daytime calibration accuracy is to compare the layer integrated attenuated backscatter (IAB) for day and night data. Assuming the nighttime data are well calibrated, the two should be reasonably close in terms of distribution and average value. Two months of IAB statistics were compared and displayed a considerable day/night difference. The average nighttime IAB for cirrus clouds was 0.027 while for daytime cirrus, the average was 0.012. For opaque water clouds, the average IAB was 0.068 and 0.026 for night and day, respectively. This difference is not necessarily due totally to calibration error per se, but is also likely related to an error in daytime background computation (too high of a background) causing the average calibrated, attenuated profile to be too vertical (slope greater than molecular). This in turn would reduce the magnitude of the calibrated attenuated backscatter within layers, especially those lower down in the profile. Regardless of the cause this analysis shows that there are still significant problems with the daytime calibration. This is an area of active investigation and it is hoped that improvements in the daytime calibration can be made for a future release.

Twilight conditions (solar elevation angle between -7° and -1°) pose the greatest problem for accurate calibration. Part of this is related to the difficulty computing the background during that time. Recall from section 2 that the background is assumed constant during night (solar elevation < -7°) and is computed from the raw photon count profile during day (solar elevation angle > -1°). In the twilight regime neither of these approaches will work. Sometimes when transitioning from day to night and in twilight, the calibration can have significant error (100%). We are currently working on improving the calibration of data acquired during both twilight and daytime conditions.

5 Layer Detection Algorithm

Included on the ATL09 data product are the top and bottom heights of cloud and aerosol layers detected in the data (ATL09 parameters *layer_top, layer_bot*) at full resolution (280 m) and the corresponding number of layers found (parameter *cloud_flag_atm*). The algorithm used to find atmospheric features within the ICESat-2 data is called the Density Dimension Algorithm (DDA-atmos). The DDA-atmos is an algorithm that has been specifically developed to analyze data collected with the ICESat-2 ATLAS instrument and processed to NRB as contained in the ATL04 data product. The need for an instrument-specific algorithm arises because ATLAS registers every photon (in the 532 nm domain of the sensor), which include signal and background (noise) photons. A challenge in signal-noise separation lies in the fact that an algorithm needs to adapt automatically to large and sometimes rapid changes in solar background. The results shown in Figure 6 demonstrate that the DDA has this capability. The DDA-atmos is part of the density-dimension algorithm family, other algorithms include an algorithm for ICESat-2 ice-surface data (the DDA-ice) and for vegetation data (the DDA-sigma-veg) (Herzfeld et al., 2014, 2017). The algorithm version used for the data analysis in this paper is described in detail in the Algorithm Theoretical Base Document for atmospheric products, part II (Herzfeld et al. 2020) and corresponds to ASAS (ATLAS Scientific Algorithm Software) code release v5.3. Data provided here are results of the standard ATL04 and ATL09 data products, release 003.

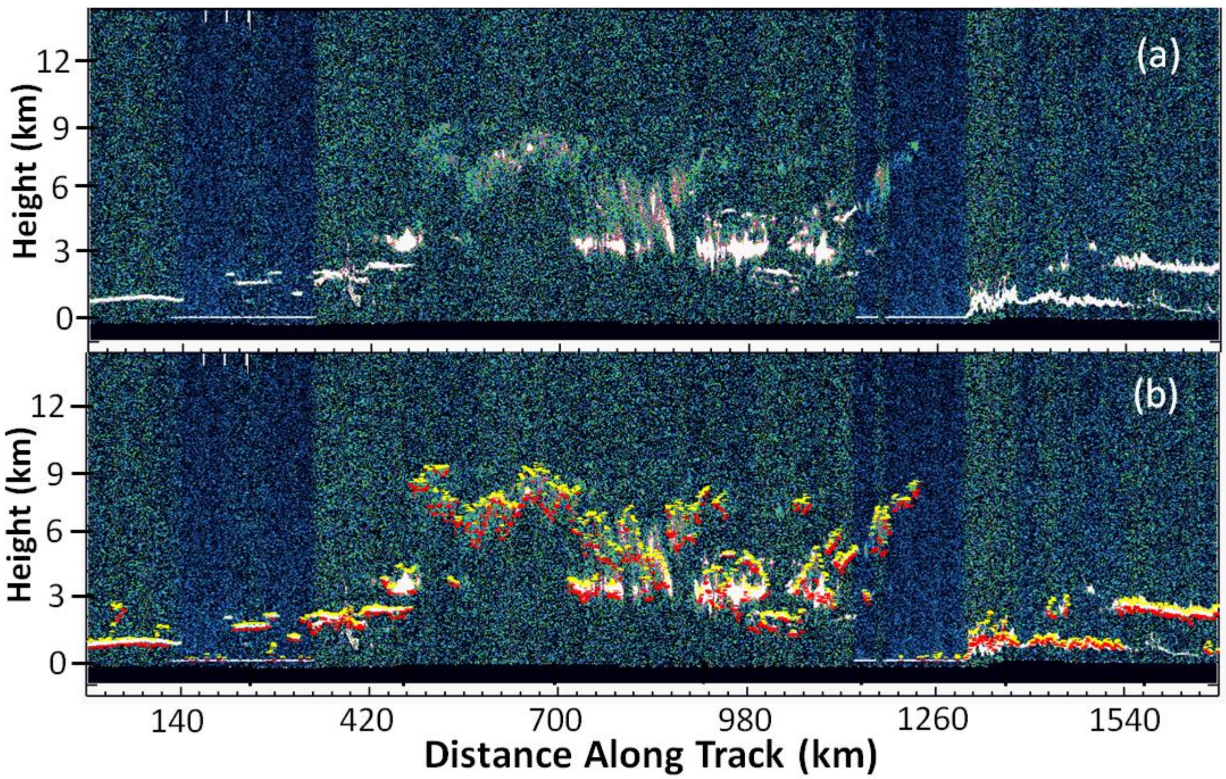

Figure 6. (a) ICESat-2 daytime attenuated backscatter image for May 27, 2020 00:35 – 00:39 UTC. (b) Same data segment as in (a), but now with the DDA layer top (yellow) and bottom (red) superimposed. Note that the DDA retrieval is not affected by the varying solar background level and the noise does not result in false positives. Data are from granule ATL09_20200527002232_09390701_003_01.h

The input to the DDA, the Normalized Relative Backscatter (NRB) data (ATL04 parameter *nrb_profile*), are arranged in a two-dimensional matrix (along track 14 km profiles). One can think of this as essentially an image of NRB. Such an image is constructed for each of the three strong laser beams, resulting in profile1, profile2, profile3. The basic concept of the DDA algorithm is a data aggregation that brings out stronger signals over weaker signals, even in locations of low signal-to-background contrast, while retaining the spatial resolution of the original input data. This data aggregation utilizes the calculation of a density field, mathematically formulated by the radial basis function (RBF). Calculation of the density field takes the role of wave-form-data analysis for pulse-limited radar and laser altimeter data, such as those from the Geoscience Laser Altimeter System (GLAS) aboard ICESat (Davis 1992, 1993, 1997); (Zwally et al. 2002); (Schutz et al. 2005). Identification of points within clouds (or other atmospheric features, such as aerosol or blowing snow layers) is motivated by the observation that a cloud is a diffuse reflector, but points within the clouds have a high probability of being located within clusters of other parts of the clouds, a property that does not hold for reflections of ambient light or noise outside of the clouds. The RBF applied here is anisotropic, because clouds typically extend more in a horizontal direction than in a vertical direction. Numerically, the density operator is a multiplication of a kernel matrix with a moving window over the data matrix. All other algorithm steps build on the calculation of the density field. Of essence are a few additional concepts: The separation of signal and noise is performed by an auto-adaptive threshold function, i.e. a statistical function that automatically adapts to the changing characteristics of the received data during different times of day and different atmospheric conditions. Because the solution of this function is determined in a space which includes density as an additional dimension, the algorithm is termed “density-dimension algorithm”. The mathematical formulation of the algorithm is given in a companion paper Herzfeld et al. (prep) and in detail in Herzfeld et al. (2020). For the user of the data product, it is only important to know that the algorithm performs the following steps, which result in matching data outputs on the ATL09 data product:

(1) Read in NRB data (NRB data are on data product ATL04)
(2) Calculate the density field (output density field, reported on product ATL09)
(3) Apply an auto-adaptive threshold function to separate signal and “noise” (background)
(4) Calculate layer boundaries and determine surface height (reported on product ATL09)

A characteristic of the ICESat-2 ATLAS instrument is that the photon count from atmospheric features can be relatively low and often not substantially exceed background values and hence the gradient between density of optically thin clouds (such as high cirrus clouds) or aerosols (from pollution or volcanic eruptions) to the surrounding atmosphere can be very small. For optically thin layers, this fact requires aggregation of data over a large neighborhood, to yield density values large enough to separate noise from atmospheric layers. For optically thick features, data aggregation over a large neighborhood is not needed (as enough points can be found in smaller neighborhoods), and also not desirable, because a larger window may introduce a larger smearing effect (depending on the coefficients in the weight matrix).

In summary, there are two objectives which suggest different controls of algorithm parameters: (1) Detection of optically thin atmospheric layers with small gradients to surrounding regions (small ratios of backscatter). (2) Precise determination of layer boundaries, wherever possible, especially for optically thick and spatially narrow layers. Both seemingly contrary goals are met by running the DDA algorithm twice with different parameters: first with a smaller window and second with a larger window (and different sigma) and combing the resultant cloud masks (layer masks). The vertical resolution of results is the same as the vertical diameter of the window; however, since the weights taper to the outside of the search window, a much higher resolution than window size is generally achieved. The effect of applying the data aggregation using density is that smaller and weaker features become more visible than in the raw data. Both density fields are reported on ATL09 and illustrated in Figure 7. The algorithm is driven by a set of so-called algorithm-specific parameters, which can be reset in case the measurement performance of the ATLAS sensor changes throughout the course of the ICESat-2 mission. The first, called layer-separation determines the minimum separation allowed for layers (meaning if less than that the layers are combined into one). The second, called layer- thickness defines the minimum thickness a layer must have in order to be reported. For release 003, these parameters have values of 4 (bins) and 20 (bins), respectively. The goal for future releases is layer-separation = 3 and layer-thickness = 3, i.e. layers are only reported if they are at least 90 m thick and separated by a 90 m gap.

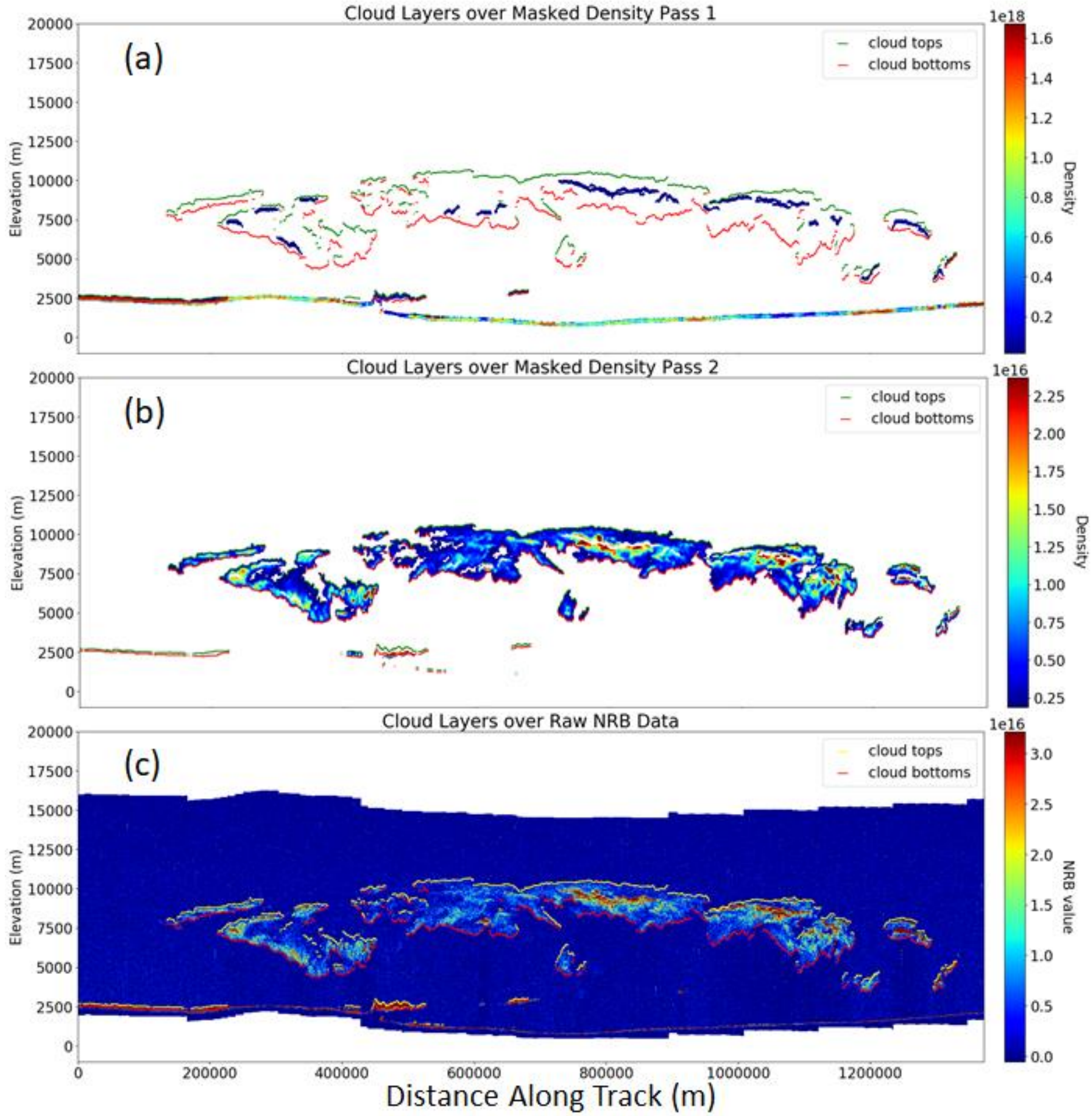

Figure 7. Output of the density calculation for pass 1 (a) and pass 2 (b). The detected layer top (yellow) and bottom (red) are overlaid on the density. Density pass 1 identifies cloud regions with higher density, whereas density pass 2 detects regions with optically thin clouds (clouds with lower density). Results from both passes are the combined into a single cloud mask, for which a layer-boundary algorithm is run and results displayed on top of the input NRB data (c).

5.1 Cloud-Aerosol Discrimination

Cloud-aerosol discrimination is a difficult problem, especially when the lidar system has only one wavelength like ICESat-2 and no depolarization channel. CALIPSO has 532 and 1064 nm channels as well as depolarization at 532 nm. In differentiating between cloud and aerosol, CALIPSO has developed a sophisticated algorithm incorporating information from all 3 of its channels. The algorithm developed for ICESat-2 must rely on information from just the one 532 channel which greatly increases the difficulty of the task. In general, clouds produce a higher backscatter signal than do aerosols. But the distribution of backscatter magnitude from clouds is not distinct from that of aerosol. The two backscatter distributions overlap and thus attenuated backscatter magnitude by itself cannot effectively be used as the sole discriminator. Other characteristics such as layer height, horizontal homogeneity, gradient of backscatter at layer top, relative humidity, etc. must be used in conjunction with signal magnitude. Aerosol transport models can also be used to help in the classification. However, no matter how sophisticated the algorithm, there will always be classification errors.

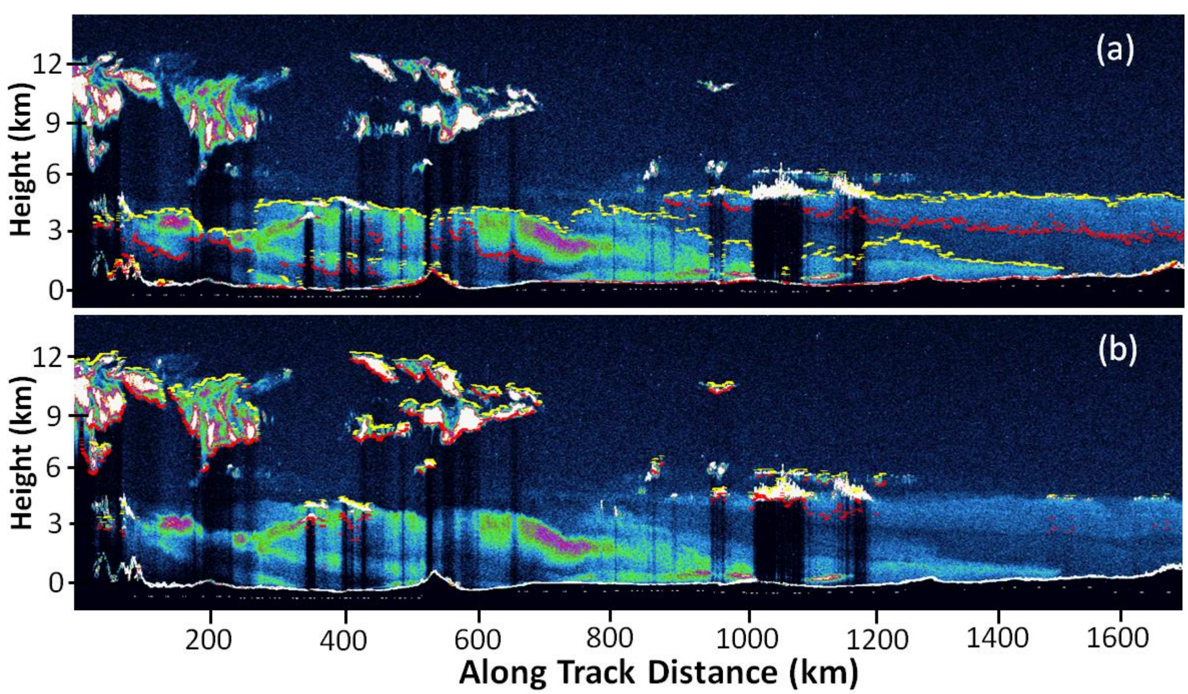

Figure 8. Cloud/aerosol discrimination algorithm output showing (a) attenuated calibrated backscatter image with only the aerosol layer top outlined in yellow and the bottom in red and

(b) showing only the top and bottom of clouds. Data shown are from October 17, 2018, granule ATL09_20181017002107_02810101_003_01.h5

The algorithm currently used for the first 3 releases (001 – 003) is very simple. The algorithm looks at the maximum attenuated backscatter within the layer and the height of the middle of the layer. If the height is greater than 6 km, then it is classified as cloud. At or below that height, if the value of the average layer scattering ratio (measured attenuated backscatter divided by attenuated molecular backscatter) is greater than 20, it is classified as cloud. If that ratio is less than 10, it is classified as aerosol. If the ratio is between these values the layer type is deemed unknown. Figure 8 shows a segment of data comprised of Saharan dust (below about 6 km) and cirrus clouds at and above 8 km.

The resulting layer discrimination (ATL09 parameter *layer_attr*) is generally correct but contains many errors in classification. We are currently working on a more sophisticated algorithm that incorporates relative humidity obtained from the GMAO product and uses a larger sample of data to statistically define the scattering ratio best able to differentiate between cloud and aerosol as a function of height and relative humidity. Further efforts to include horizontal and vertical homogeneity and GEOS-5 model analysis of aerosol location are also being pursued. We anticipate having a better cloud/aerosol discrimination routine for the release 004 data products now scheduled for release in early 2021.

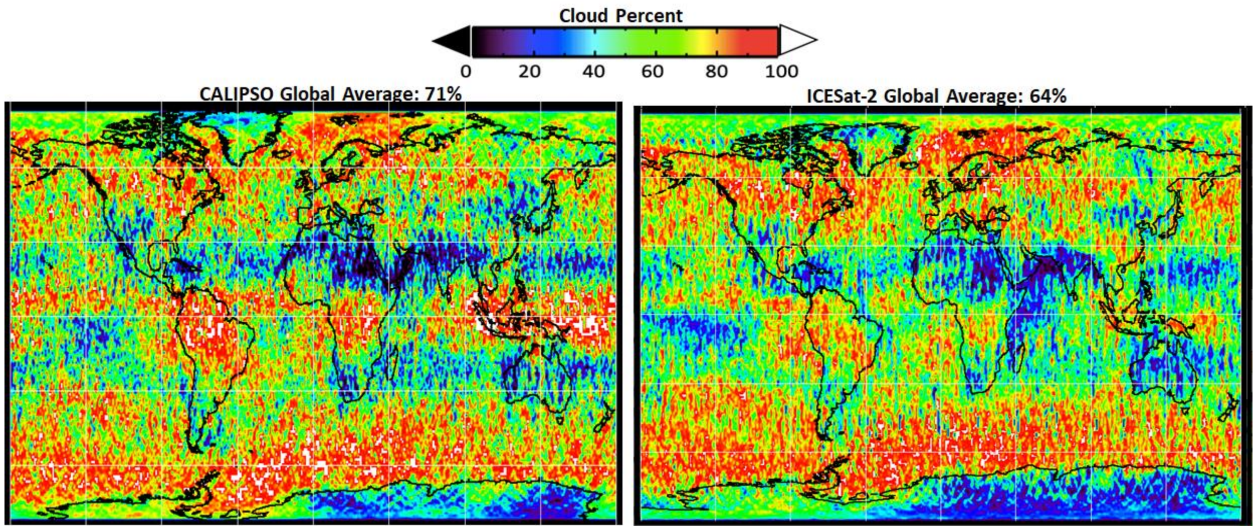

Figure 9. A comparison of global cloud distribution as derived from CALIPSO (left) and ICESat-2 DDA (right) for November 2018. Outside of the tropical region, both measurements agree very well.

One way to ascertain the performance of the DDA and the cloud/aerosol discrimination algorithm is to compare ICESat-2 and CALIPSO global cloudiness. Figure 9 shows the distribution of cloud occurrence derived from CALIPSO (left) and ICESat-2 (right) for November 2018. Outside of the tropics, the two measurements agree quite well. In the region near the equator, the ICESat-2 cloud fraction is considerably less than CALIPSO. This is undoubtedly due to the fact that many of the clouds there reach heights > 14 km. ICESat-2 is blind to clouds that occur between the altitudes of 14 – 15 km and clouds above 15 km are folded down to the bottom of the profile (as discussed in the introduction). Thus, it is not surprising that there are large discrepancies in the tropics. Figure 10 shows the November 2018 zonal cloud fraction from CALIPSO (green line) and ICESat-2 DDA retrievals (solid black line) along with the cloud detection method based on Apparent Surface Reflectance (ASR) (dashed black line) which is explained in section 7.1. The red line is the CALIPSO zonal cloud fraction for clouds below 14 km.

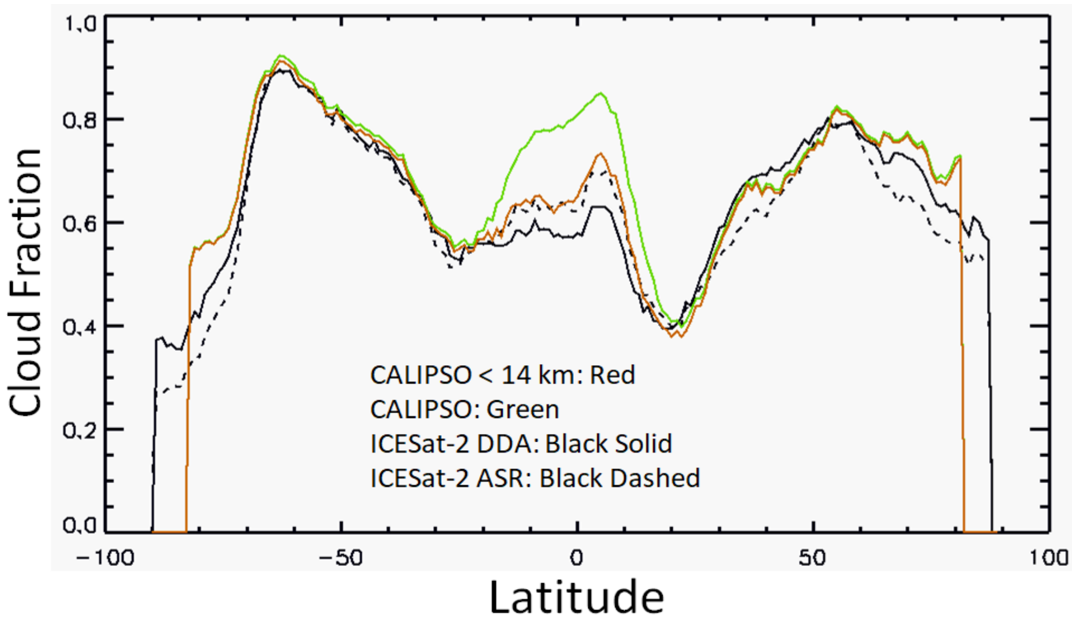

Figure 10. November 2018 zonal average cloud fraction for CALIPSO (green), ICESat-2 from the DDA (black solid) and the ASR method of cloud detection (black dashed). The red line is CALIPSO detected clouds below 14 km altitude.

6 Blowing Snow

One of the main reasons that ICESat-2 acquires atmospheric data is to aid the analysis of altimetric data. Multiple scattering of the laser pulse as it travels through clouds, fog and blowing snow can cause significant error in altimetry measurements (Duda et al., 2001, Yang et al. 2010*)*. The lower and optically denser a layer is, the larger the problem. Blowing snow, because it is so prevalent over Antarctica and always occurs right at the ground, creates a large multiple scattering effect and can produce the largest altimetry error (reducing the measured surface height by up to 10's of cms). Hence, detection of blowing snow is very important for flagging and or filtering of altimetry data that may be affected.

The ATL09 data product gives the height and optical depth of any detected blowing snow layers at both high (25 Hz) and low (1 Hz) resolution (ATL09 parameters *bsnow_h and bsnow_od*, respectively). The blowing snow detection algorithm is invoked over any surface that is identified as snow covered, land ice or sea ice. The algorithm looks at the calibrated, attenuated backscatter value in the bin above the identified surface bin. If the scattering level in that bin is greater than 10 times the molecular value and the 10 m wind speed is greater than 4 m/s, the scattering value of each successive bin above that bin is checked to see if it falls below 8 times the molecular value (in search of the layer top). If this has occurred for two consecutive bins and the thickness of the layer is less than 500 m, then the layer is considered as blowing snow. If the top of the layer has not been found within 500 m of the surface, the layer is identified as diamond dust (i.e. not considered blowing snow). In this case, a flag is set to indicate the likely presence of diamond dust.

The optical depth of the layer is computed assuming an extinction to backscatter ratio of 25 through the layer. The blowing snow detection algorithm is very similar to that described in Palm et al., (2011 and 2018) that was extensively used to retrieve blowing snow over Antarctica from CALIPSO data for the period 2006 – 2017. For further details on the algorithm please see Palm et al., (2020). An example of blowing snow detected by the algorithm over Antarctica is shown in Figure 11. Figure 11a and b show the blowing snow frequency over Antarctica for the months of April and May 2019. Figure 11c shows the attenuated backscatter for a portion of one track across Antarctica with the layer top (parameter *bsnow_h*) indicated by the yellow dots. The backscatter image shown in Figure 11c is very typical of wintertime blowing snow layers in Antarctica, some of which can stretch for over 2000 km and reach heights of 400 m (Palm et al., 2018).

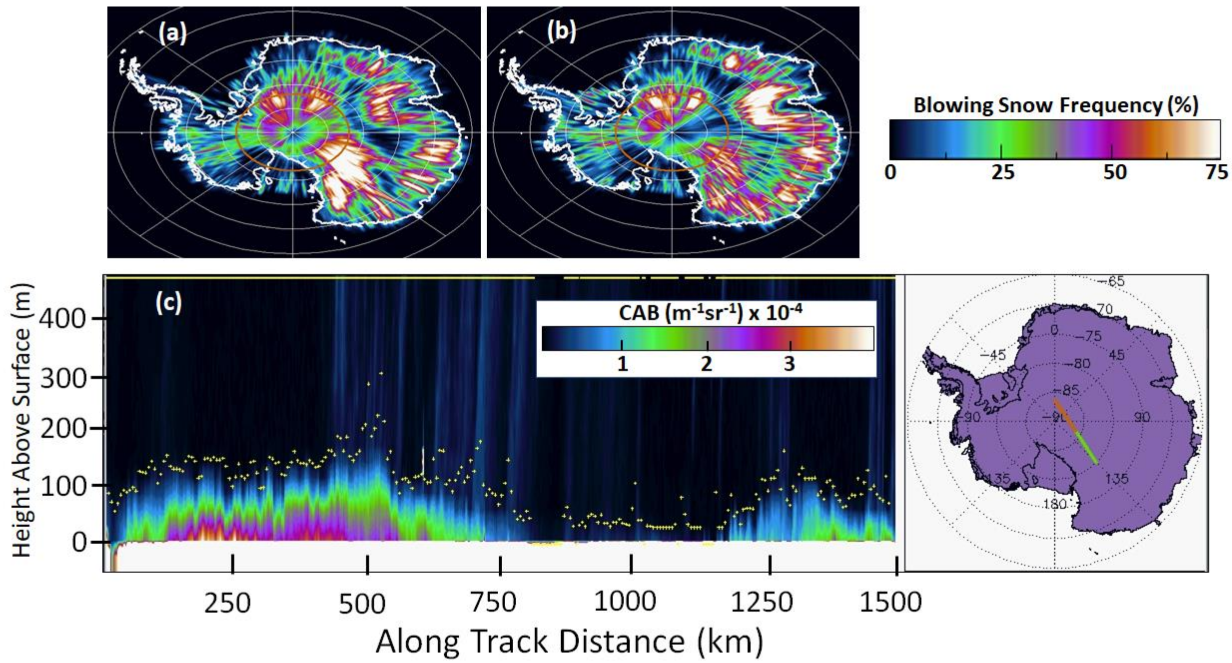

Figure 11. Blowing snow frequency for the months of April (a) and May (b), 2019. (c) ICESat-2 calibrated attenuated backscatter (CAB) along the track shown on the map with blowing snow layer top indicated by the yellow dots. The green part of the track corresponds to the left half of the image and red the right half. Data in (c) are from granule ATL09_20190420074102_03370301_003_01.h5

7 Apparent Surface Reflectance

The Apparent Surface Reflectance (ASR) is essentially the ratio of received laser energy reflected from the surface to the transmitted energy (Yang et al., 2013). The ASR depends on two things: the actual reflectivity of the surface and the two-way transmission of the atmosphere between the surface and the satellite. In a perfectly clear (molecular only) atmosphere over a surface with a reflectivity of 1.0, the ASR would be about 0.80 (the two-way transmission of a molecular atmosphere at sea level). Mathematically, the ASR (ρ_{app}) is defined as

$$\rho_{app} = \frac{\pi N_p r^2 D_c F}{N E A_t S_{ret}} \quad (9)$$

where N_p is the number of photons received from the surface, r is the distance between the satellite and the surface, D_c is the detector dead time correction factor, F is a calibration factor, E is the laser pulse energy, A_t is the area of the telescope, and S_{ret} is the product of the transmittance of the optics and the quantum efficiency of the detector, and N is the number of laser pulses summed (400). The calibration factor (F) was obtained by analyzing many (clear) ICESat-2 passes over the Antarctic Plateau, and assuming a surface reflectance of 1 and a two-way atmospheric transmission of 0.85. The ASR is computed globally and of course is only defined when there is a detectable surface signal. It is stored on the ATL09 data product as parameter *apparent_surf _reflec*.

An example of global ASR for the month of January 2019 is shown in Figure 12. This figure is taken from the ATL17 data product which contains the monthly gridded fields of many of the atmospheric parameters that reside in the ATL09 data product. Over the ocean and snow-free land surfaces, the ASR has a small range of about 0.05 to 0.3. The snow and ice-covered areas in the northern hemisphere have ASR values in the 0.4 to 0.6 range, while over parts of East Antarctica, the ASR reaches close to 0.8. Note that there has been no attempt to cloud clear the data when compiling the data shown in Figure 12, and thus the atmospheric attenuation from clouds, aerosols and air molecules is included in these data and will decrease the average ASR values.

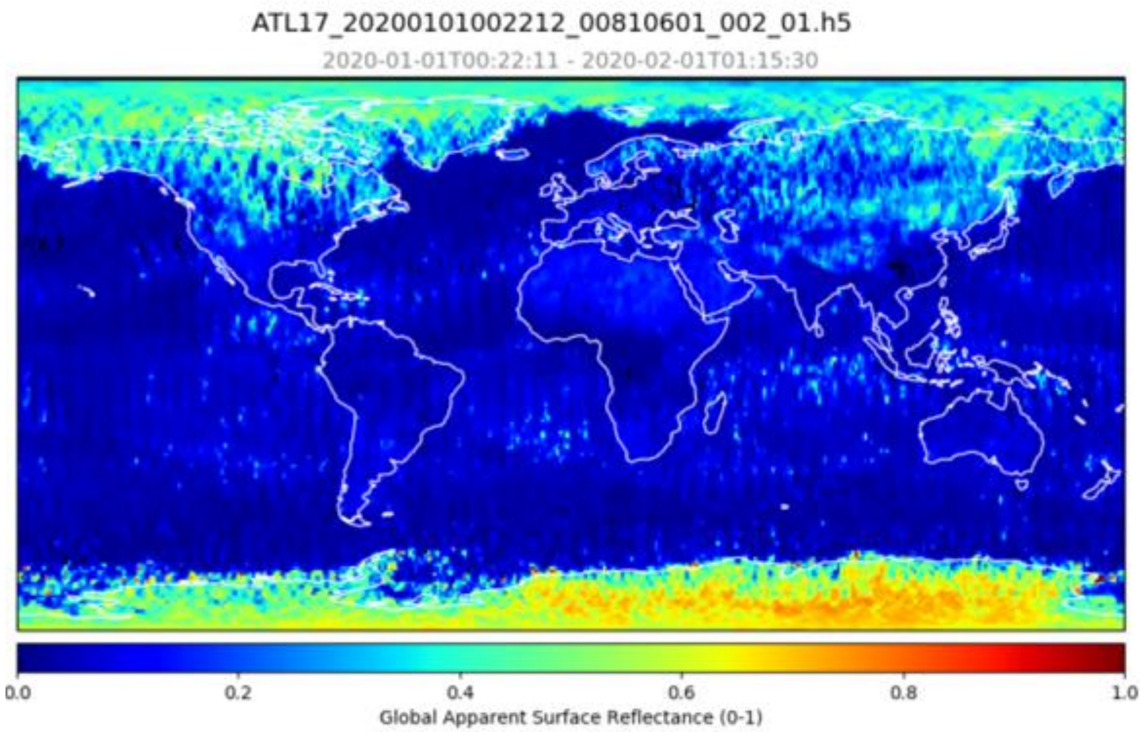

Figure 12. ICESat-2 measured global Apparent Surface Reflectance (ASR) for the month of January 2020.

7.1 Cloud Detection using ASR

Since the ASR is dependent on the two-way transmission of the atmosphere, it can be used to infer the presence of clouds. However, this is only possible if the actual reflectivity of the surface at 532 nm (R_{surf}) is known sufficiently well. In fact, the accuracy of such retrievals depends directly on the accuracy of the assumed surface reflectivity. Over land we use the monthly surface reflectivity data derived from the *Global Ozone Monitoring Experiment-2* (GOME-2) and the SCanning Imaging Absorption SpectroMeter for Atmospheric CHartographY (SCIAMACHY) missions (Tilstra et al. 2017). This global data set provides the average surface reflectivity at a resolution of 0.25x0.25 degree for each month of the year. An example of these data is shown in Figure 13 for January and July. In addition, we also use the NOAA daily snow and ice cover data et (global, 0.04x0.04 degree resolution) derived from the combined observations from METOP, AVHRR, MSG SEVIRI, GOES and DMSP SSMIS. If the surface is snow covered land we assume the surface reflectivity is 0.60.

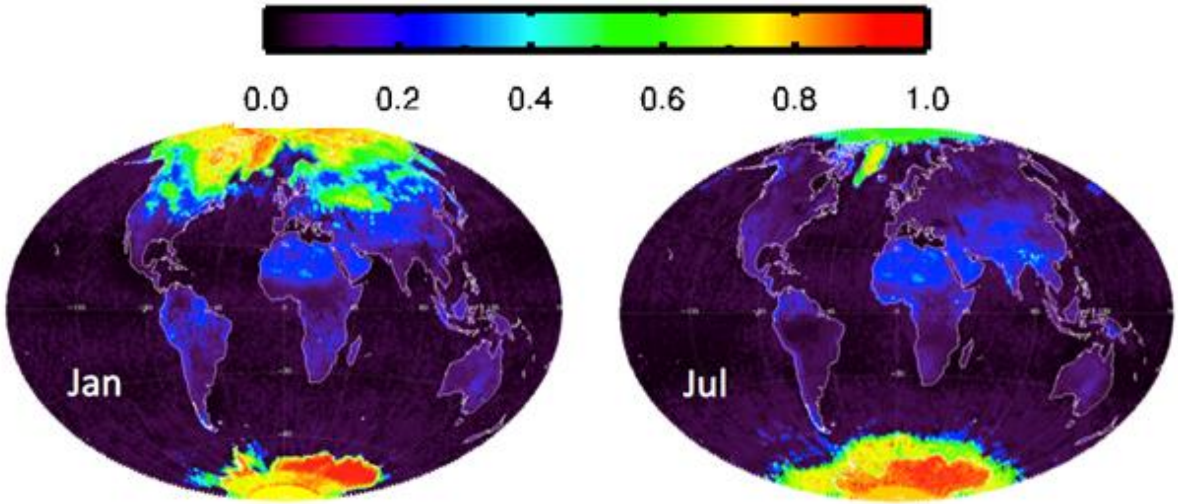

Figure 13. The monthly 532 nm surface reflectivity climatology derived from the GOME data for January and July. Data from http://www.temis.nl/surface/gome2_ler.html

Over ocean and inland water bodies we use the method of Lancaster et al. (2005) to compute the surface reflectance from surface wind speed. The reflectance (*R*) of the ocean's surface is described by:

$$R = (1 - W)R_s + WR_f \tag{10}$$

Where R_s is the Fresnel reflectance from the surface, R_f is the reflection due to whitecaps and W is the fraction of the surface covered by whitecaps. Here we use $R_f = 0.22$ as the Lambertian reflectance of typical oceanic whitecaps at a wavelength of 532 nm (Koepke, 1984). Following Bufton et al. (1983), the Fresnel reflectance (R_s) is

$$R_s = \frac{\rho}{4\langle S^2 \rangle} \tag{11}$$

Where ρ is the Fresnel reflection coefficient and $\langle S^2 \rangle$ is the variance of the distribution of wave slopes. The Fresnel reflection coefficient is a function of wavelength and is computed as ρ =

0.0205 at 532 nm, from the tabulations of Hale and Querry [1973]. Cox and Munk (1954) provide an empirical description of $\left\langle S^2 \right\rangle$ as a function of wind speed:

$$\langle S^2 \rangle = 0.003 + 5.12x10^{-3} U_{12.4} \qquad (12)$$

Where $U_{12.4}$ is the wind speed at 12.4 m above the ocean surface. Numerical weather prediction models generally output wind speed at the 10 m height which can be adjusted to the 12.4 m level assuming neutral atmospheric stability.

$$U_{12.4} = U_{10} \left(\frac{12.4}{10.0}\right)^{0.143} \qquad (13)$$

In computing the ocean lidar return from whitecaps the relative area of the ocean surface that they cover is estimated from the relation from Monahan and O'Muircheartaigh (1980):

$$W = 2.95x10^{-6} U_{10}^{3.52} \qquad (14)$$

The algorithm used to determine the presence of cloud from a given measurement of ASR sets a threshold (T_{hresh}) based on the value of the surface reflectance (R_{surf} computed as described above for land or water) at the current location times the molecular two-way transmittance times an adjustable factor (ϕ - currently 1.0 over water and 1.1 over land):

$T_{hresh} = R_{surf} * \phi * (T_m)^2$

Where $(T_m)^2$ is the two-way 532 nm molecular transmission (nominally 0.81 at sea level). A probability (P) of cloud occurrence is then computed as:

$P = (1 – ASR/T_{hresh}) * 100$

We have found that values of P > 60 agree well with cloud occurrence as determined from the DDA analysis of backscatter. The value of P is stored on the ATL09 product (parameter *asr_cloud_probability*) as is a flag (parameter *cloud_flag_asr*) to indicate the likely presence of a cloud (P > 60). Figure 14 shows the comparison of cloud detection by this (ASR) method and that using the DDA for the month of May 2019. The total global average cloud fraction determined from the DDA (0.67) is very close to that of the ASR method (0.63).

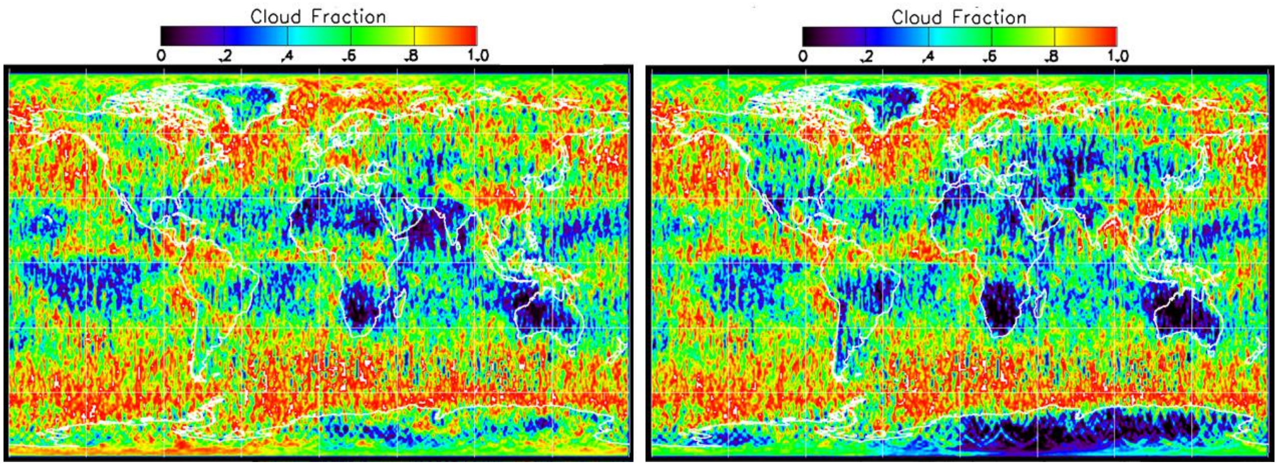

Figure 14. Cloud fraction for May 2019 as determined from the DDA analysis of backscatter (left panel) and the cloud fraction as determined from the ASR cloud detection method (right panel, P > 60).

Prior to launch, model results indicated that the lower limit for the ASR method of cloud detection would be optical depths in the range 0.2 to 0.4. After launch we have not yet quantified this limit through data analysis, but the results of Figure 14 indicate that we are probably meeting or exceeding that value. However, one must remember that the ASR method of cloud detection does not have the ability to differentiate between cloud and aerosol, and this method will inadvertently include thicker aerosol layers.

7.2 Total Column Optical Depth from ASR

The total atmosphere column particulate (not including molecular) optical depth can be computed from the apparent surface reflectance if the actual surface reflectance is well known. This condition holds over ocean where the surface reflectance can be computed from wind speed and over known surfaces like Antarctica and the interior of Greenland. Of course, for this method to be applicable, the surface return cannot be totally attenuated (zero). Thus, this technique is limited to cases where the overlying cloud and aerosol have a combined optical depth of less than about 3. Above that limit, the surface signal will be too small to be detected or totally attenuated. Here we will only consider data over the ocean or inland water bodies.

In the ensuing discussion, let the ASR be called R_{app} and the ocean or water reflectance R_{true}. R_{app} must be corrected for molecular attenuation and the angle with which the laser beam makes with nadir (Θ):

$$R_{cor} = (R_{app})/(cos(\theta)\bar{T}_m^2) \qquad (15)$$

where R_{cor} is the resultant corrected reflectance, Θ is the tilt angle of the lidar with respect to nadir viewing (normally 0.1 degree but can reach 5.0 degrees and may vary with laser beam), and $\bar{T}_m^2$ is the mean molecular two-way transmission for the entire atmospheric column at 532 nm (~0.81 at sea level). The relationship between the corrected observed ATLAS reflectance (R_{cor}) and the modeled surface reflectance (R_{true}) is described below:

$$R_{cor} = R_{true}e^{-2\tau} \qquad (16)$$

where τ is the optical depth of the particulates (cloud plus aerosol) in the atmospheric column. Solving for τ results in the equation:

$$\tau = -\frac{1}{2}ln(R_{cor}/R_{true}) \qquad (17)$$

The column optical depth is ATL09 parameter *column_od_asr* and an example of the retrieval over ocean for the month of January 2020 is shown in Figure 15.

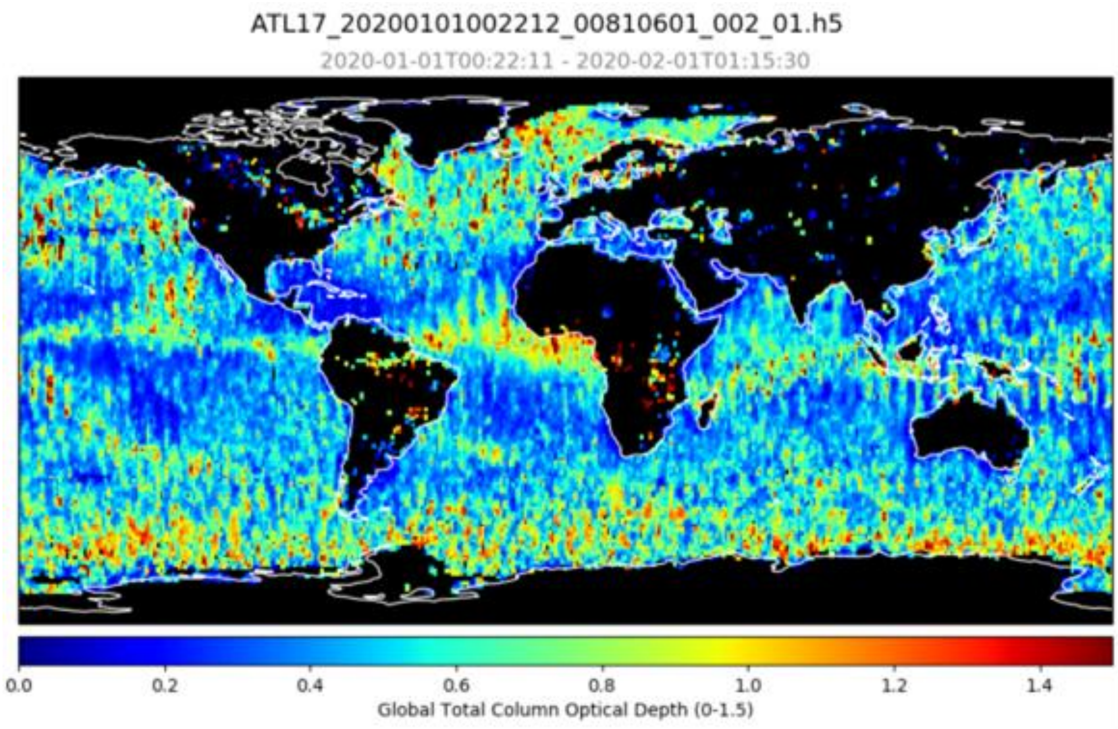

Figure 15. Average total column optical depth over ocean and inland water bodies for the month of January 2019. Note that the column optical depth can only be computed when the surface signal is detected, and thus the upper limit of these retrievals is about 3.

8 Summary and Conclusion

ICESat-2 was launched in September of 2018 and has been acquiring data continuously since October 13, 2018. While primarily a mission to obtain high resolution measurements of the earth's topography and monitor changes in the height of ice sheets and sea ice thickness, ICESat-2 also acquires profiles of atmospheric backscatter. The optimization of the ATLAS instrument for altimetry imposes various limitations on the atmospheric data. The high repetition rate (10 KHz), low per pulse energy (100 μJ) laser restricts the atmospheric backscatter profiles to just 14 km in height and results in poor daytime signal to noise. The restricted vertical range makes computation of background and calibration much more difficult than in other satellite lidars such as GLAS or CALIOP. However, the first of its kind (for a satellite lidar) Telescope Alignment Monitoring System (TAMS) keeps the laser footprint within the telescope field of view thereby keeping the calibration remarkably steady. Results indicate that the nighttime calibration is very stable and the data can be accurately calibrated to within 5-10%. There are still problems with the daytime and twilight calibration which can have considerable error (especially twilight). The daytime calibration value is roughly twice that of the night value and appears to be related to the magnitude of the solar background. Data with higher background tends to have a lower calibration value and vice versa. In addition, atmospheric features above 14 km are not detected and scattering above 15 km at height z is folded down to a height of z - 15 km. Thus, a cloud at 16 km will be seen at 1 km height and be added to the scattering that is present there. This usually occurs only in the tropics and we have attempted to flag such occurrences in the ATL09 data product (parameter *cloud_fold_flag*).

Table 2. A list of the ATL09 data parameters discussed in the text. The "x" in "profile_x"stands for the 3 beams or profiles (i.e. x=1,2,3)

ATL09 Product Parameter profile_x/high_rate/	Description	Units	Horizontal/Vertical Resolution(m)
cab_prof	Calibrated, attenuated backscatter profile	$m^{-1}sr^{-1}$	280/30
layer_top/layer_bot	Layer top/bottom height (maximum of 10 layers)	m	280/30
layer_attr	Layer type: 1,2,3: cloud, aerosol, unknown	NA	NA
cloud_flag_atm	Number of layers detected (0-10)	NA	NA
asr_cloud_probability	The probability (0-100) of a cloud being present based on the magnitude of ASR	NA	280/NA
cloud_flag_asr	0 (low)-5 (high) flag indicating cloud probability based on ASR	NA	280/NA
bsnow_h	Blowing snow layer depth	m	280/30

bsnow_od	Optical depth of blowing snow layer if detected	NA	280/NA
apparent_surf_relec	Apparent Surface Reflectance (ASR)	NA	280/NA
column_od_asr	Total column optical depth	NA	280/NA
cloud_fold_flag	A flag indicating the profile likely contains a cloud above 15 km that has been folded down	NA	280/NA

The Density Dimension Algorithm (DDA) is used to locate atmospheric features in the data at full resolution (no horizontal averaging). The technique is auto-adaptive, meaning it can adapt to rapidly changing background noise conditions. In addition, unlike algorithms used in previous satellite lidars, the DDA does not require calibrated backscatter to locate layer boundaries. This was a main reason for selecting the DDA for use with ICESat-2 data, since prior to launch it was not known how well the data could be calibrated. Results show that the DDA is performing very well both day and night. Daytime detection of layers is hindered by the large magnitude of solar background noise, but the DDA is still able to retrieve most clouds and some thicker aerosol. False positives do not appear to be a problem, but the algorithm does miss some very tenuous layers even at night. Future releases will improve the detection of optically thin layers. Currently, the cloud/aerosol discrimination routine is too simplistic and efforts are underway to improve this for the next release due out in early 2021.

The blowing snow detection algorithm that was designed for and used with CALIPSO data was adapted for use with ICESat-2 data and shows promising results on par with the CALIPSO measurements summarized in Palm et. al., (2018). These data will enable us to extend the blowing snow climatology that work began, which covers the period 2006 - 2017. The blowing snow product contains the height and estimated optical depth of any blowing snow layer detected over a snow covered, ice covered or sea ice surface as indicted by ancillary data such as the NOAA daily global snow cover data set. In addition, the blowing snow retrievals are aiding the altimetry mission by locating layers that can cause multiple scattering induced range delay, which causes the measured surface height to be too low.

Apparent Surface Reflectivity (ASR) can be used to determine the likely presence of a cloud if a reasonable estimate of the true surface reflectance is known. Over ocean, the surface reflectance is a function of surface wind speed and can be computed from the method of Cox and Munk (1954). Comparison of this method of cloud detection with direct detection from backscatter using the DDA shows good agreement. The ASR can also be used to compute total column optical depth since the measured ASR is a function of both the surface reflectivity and the two-way atmospheric transmission. However, as with cloud detection using ASR, the true surface reflectivity must be known. While never known perfectly, estimates of surface reflectivity are most accurate over water bodies due to its dependence on wind speed. Retrievals over land are more error prone since the surface reflectivity changes on temporal and spatial scales smaller than the resolution of current databases.

In conclusion, though ICESat-2 was not designed as an atmospheric mission, it is acquiring valuable atmospheric data on clouds, aerosols and blowing snow. These data are currently providing additional coverage to the existing lidars in space such as CALIPSO and Aeolus. In addition, the precessing orbit of ICESat-2 can give information on the diurnal cycle of cloud occurrence and structure, something that a lidar in a sun-synch orbit cannot do. The processing of ICESat-2 atmospheric data is challenging, but the work presented here has demonstrated that these challenges can be overcome. While problems still exist (mainly with calibration and possibly background computation), we are confident that future work will continue to increase the accuracy and utility of the ICESat-2 atmospheric data products. In particular we are hopeful that layer extinction and optical depth for at least the nighttime data can be included in a future release of the data products.

Acknowledgements and Data

The authors would like to thank the NASA ICESat-2 project office for funding this work and members of the ATLAS Science Algorithm Software (ASAS) development team who create the software to produce the atmospheric data products. Thanks also to the ICESat-2 Science Investigator-led Processing System (SIPS) team that produce the actual data products and the ATLAS Instrument Support Team that manages flight operation of the ATLAS instrument.

The data presented in this paper are freely available at the National Snow and Ice Data Center (NSIDC). Visit https://nsidc.org/data/icesat-2/data-sets to obtain the ICESat-2 atmospheric data products and documentation. The atmospheric products discussed in this paper are ATL04 – Normalized Relative Backscatter (NRB) profiles, ATL09 – calibrated attenuated backscatter profiles and layer characteristics, ATL16 – weekly gridded atmosphere products and ATL17 – monthly gridded atmosphere products. All data product files are in hdf5 format.

References

Abdalati, W. et al. (2010) The ICESat-2 Altimetry Mission. *IEEE Transactions on Geoscience and Remote Sensing,* **98**, **5**, 735 – 751. **DOI:** 10.1109/JPROC.2009.2034765

Bufton, J.L., F.E. Hoge and R.N. Swift, (1983), Airborne measurements of laser backscatter from the ocean surface. *Appl. Opt*., **22, 17**, https://doi.org/10.1364/AO.22.002603

Cox, C. and W. Munk, (1954), Measurement of the Roughness of the Sea Surface from Photographs of the Sun's Glitter. *J. Opt. Soc. Am*. **44**, 838-850

Davis, C. H. (1992). Satellite radar altimetry. Microwave Theory and Techniques, *IEEE Transactions on Geoscience and Remote Sensing*, 40(6):1070-1076

Davis, C. H. (1993). A surface and volume scattering retracking algorithm for ice sheet satellite altimetry. *IEEE Transactions on Geoscience and Remote Sensing* 31(4):811-818.

Davis, C. H. (1997). A robust threshold retracking algorithm for measuring ice-sheet surface elevation change from satellite radar altimeters. *IEEE Transactions on Geoscience and Remote Sensing*, 35(4):974-979.

Duda, D.P., J. D. Spinhirne, and E.W. Eloranta (2001), Atmospheric multiple scattering effects on GLAS altimetry – part I: Calculations of single path bias, *IEEE Trans. Geos. Rem. Sens.*, *39*, 92-101.

Hale, G.M. and M.R. Querry, (1973), Optical constants of water in the 200-nm to 200-µm wavelength region. *Appl. Opt*., **12, 3**, https://doi.org/10.1364/AO.12.000555

Herzfeld, U., Palm, S., and Hancock, D. (2020). ICESat-2 Algorithm Theoretical Basis Document for the Atmosphere, Part II: Detection of Atmospheric Layers and Surface Using a Density Dimension Algorithm, v11.0, https://doi.org/10.5067/TE10T7E5TNGK

Herzfeld, U., Palm, S., Hancock, D., and Hayes, A. (prep). Detection of thin clouds, aerosols, blowing snow and other tenuous atmospheric layers in ICESat-2 ATLAS data and their relevance in climate models. *Geophys. Res. Lett*

Herzfeld, U., Trantow, T., Harding, D., and Dabney, P. (2017). Surface-height determination of crevassed glaciers | Mathematical principles of an Auto-Adaptive Density-Dimension Algorithm and validation using ICESat-2 Simulator (SIMPL) data. *IEEE Transactions in Geoscience and Remote Sensing*, 55(4)

Herzfeld, U., McDonald, B., Wallin, B., Markus, T., Neumann, T., and Brenner, A. (2014). An algorithm for detection of ground and canopy cover in micropulse photon-counting lidar altimeter data in preparation of the ICESat-2 mission. *IEEE Transactions Geoscience and Remote Sensing*, 54(4).

Koepke, P., (1984), Effective reflectance of oceanic whitecaps. *Appl. Opt*., **23, 11**, https://doi.org/10.1364/AO.23.001816

Lancaster, R.S., J.D. Spinhirne and S.P. Palm, (2005), Laser pulse reflectance of the ocean surface from the GLAS satellite lidar. *Geophys. Res. Lett*. **32, 22**, https://doi.org/10.1029/2005GL023732

Markus, T., T. Neumann, A. Martino, W. Abdalati, K. Brunt, B. Csatho, S. Farrell, H. Fricker, A. Gardner, D. Harding, M. Jasinski, R. Kwok, L. Magruder, D. Lubin, S. Luthcke, J. Morison, R. Nelson, A. Neuenschwander, S. Palm, S. Popescu, C.K. Shumj, B. E. Schutz, B. Smith, Y. Yang, J. Zwally (2017) The Ice, Cloud, and land Elevation Satellite-2 (ICESat-2): Science requirements, concept, and implementation. *Remote Sens. Environ.* 190, 260–273, http://dx.doi.org/10.1016/j.rse.2016.12.029

Martino, A., J., T. A. Neumann, N. T. Kurtz, and D. McClennan, (2019), ICESat-2 Mission Overview and Early Performance. Proc. SPIE 11151, Sensors, Systems, and Next-Generation Satellites XXIII, 111510C (10 October 2019); https://doi.org/10.1117/12.2534938

McGill, M., D. Hlavka, W. Hart, V.S. Scott, J. Spinhirne and B. Schmid, (2002), Cloud physics lidar: Instrument description and initial measurement results. *Appl. Opt*., **41, 18**, 3725-3734, https://doi.org/10.1364/AO.41.003725

Monahan,E.C. and I. Muircheartaigh, (1980), Optimal power-law description of oceanic whitecap dependence on wind speed. *J. Phys. Oceanogr*., **10**, 2094-2099. https://doi.org/10.1175/1520-0485(1980)010%3C2094:OPLDOO%3E2.0.CO;2

Palm, S. P., Y. Yang and U. Herzfeld (2020): Ice, Cloud, and Land Elevation Satellite (ICESat-2) Project Algorithm Theoretical Basis Document for the Atmosphere, Part I: Level 2 and 3 Data Products, version 3 https://doi.org/10.5067/X6N528CVA8S9

Palm, S. P., Kayetha, V., & Yang, Y. (2018). Toward a satellite-derived climatology of blowing snow over Antarctica. *Journal of Geophysical Research: Atmospheres*, 123, 10,301–10,313. https://doi.org/10.1029/2018JD028632

Palm, S. P., Yang, Y., Spinhirne, J. D., & Marshak, A. (2011). Satellite remote sensing of blowing snow properties over Antarctica. *Journal of Geophysical Research: Atmospheres*, *116*(D16), D16123. https://doi.org/10.1029/2011JD015828.

Pauly, R. M., J. E. Yorks, D. L. Hlavka, M. J. McGill, V. Amiridis, S. P. Palm, S. D. Rodier, M. A. Vaughan, P. A. Selmer, A. W. Kupchock, H. Baars, and A. Gialitaki (2019), Cloud-Aerosol Transport System (CATS) 1064nm calibration and validation *Atmos. Meas. Tech*., 12, 6241–6258, https://doi.org/10.5194/amt-12-6241-2019

Schutz, B., Zwally, H., Shuman, C., Hancock, D., and DiMarzio, J. (2005). Overview of the ICESat Mission. *Geophys. Res. Lett.*, 32(21).

Spinhirne, J.D., S.P. Palm, W.D. Hart, D.L. Hlavka and E.J. Welton, (2005) Cloud and aerosol measurements from GLAS: Overview and initial results. *Geophys. Res. Lett*., **32, 22**, https://doi.org/10.1029/2005GL023507

Tilstra, L. G., Tuinder, O. N. E., Wang, P., and Stammes, P.: Surface reflectivity climatologies from UV to NIR determined from Earth observations by GOME-2 and SCIAMACHY, *J. Geophys. Res.-Atmos*., 122, 4084–4111, 2017.

Winker, D. M., Vaughan, M. A., Omar, A., Hu, Y. X., Powell, K. A., Liu, Z. Y., et al. (2009). Overview of the CALIPSO mission and CALIOP data processing algorithms. *Journal of Atmospheric and Oceanic Technology*, *26*(11), 2310-2323. https://doi.org/10.1175/2009jtecha1281.1

Yang, Y., A. Marshak, T. Varnai, W. Wiscombe, P. Yang, 2010: Uncertainties in Ice-Sheet Altimetry From a Spaceborne 1064-nm Single-Channel Lidar Due to Undetected Thin Clouds. *IEEE Trans. Geos. Remote Sens.,* 48, 250-259.

Yang, Y., A. Marshak, S. Palm, Z. Wang, C. Schaaf, 2013: Assessment of Cloud Screening with Apparent Surface Reflectance in Support of the ICESat-2 Mission. *IEEE Trans. Geos. Remote Sens*., 51(2), 1037-1045, doi: 10.1109/TGRS.2012.2204066.

Zwally, H., Schutz, B., Abdalati, W., Abshire, J., Bentley, C., Brenner, A., Bufton, J., Dezio, J., Hancock, D., Harding, D., Herring, T., Minster, B., Quinn, K., Palm, S., Spinhirn, J., and Thomas, R. (2002). ICESat's laser measurements of polar ice, atmosphere, ocean, and land. *Journal of Geodynamics*, 34(3-4):405{445.